

## Quantifying porewater exchange across the sediment-water interface in the deep sea with in situ tracer studies

Alexandra M. F. Rao and Richard A. Jahnke

Skidaway Institute of Oceanography, 10 Ocean Science Circle, Savannah, GA 31411, USA

### Abstract

A numerical model of NaBr tracer transport in benthic flux chamber incubations has been developed to simulate temporal changes in chamber water tracer concentrations and applied to four deep sea locations: the California and North Carolina margins, the Ceara rise, and the Cape Verde plateau. Model variables include the chamber volume (which determines the initial tracer concentration), and rates of diffusive and nonlocal exchange across the sediment-water interface. Chamber volume and solute exchange rate estimates were obtained by optimizing the fit between observations and model results using a  $\chi^2$  statistical scheme. We observe enhanced solute exchange in regions with high organic carbon rain rates, over a wide range of bottom water oxygen concentrations. Furthermore, our results demonstrate that solute exchange rates cannot be assumed constant, even within relatively short deployments. In six of 22 cases, chamber volumes and corresponding benthic solute fluxes derived from model fits were more than 20% greater than values calculated using linear extrapolations of chamber tracer concentration-time relationships. To avoid this discrepancy, future benthic chamber studies should seek to minimize the time interval between tracer injection and sampling while maintaining sufficient time to achieve complete homogenization of the tracer in the chamber waters.

**Background**—Benthic chamber incubations and porewater gradient calculations are established techniques for assessing benthic fluxes of oxidants, microbial metabolites, and products of mineral dissolution and precipitation in sediments. The accuracy of benthic solute flux estimates derived from in situ flux chamber incubations depends on an accurate assessment of the volume of water incubated in each chamber, whereas solute flux estimates from porewater gradient calculations require the knowledge of the rates and mechanisms governing solute exchange. Benthic solute exchange between bottom water and porewater in low-permeability sediments occurs by molecular diffusion across the sediment-water interface (SWI) and across irrigated macrofaunal burrow walls (bioirrigation, nonlocal exchange), as well as by bioturbation—biological sediment and porewater mixing near the SWI (Aller 1990; Jahnke et al. 1986; Meile et al. 2001; Schlüter et al. 2000).

Previous studies have estimated solute exchange rates by comparing porewater diffusion calculations and in situ ben-

thic chamber measurements (Glud et al. 1994; Archer and Devol 1992). These rates have also been estimated using whole core incubations with solute tracers (Martin and Banta 1992), and in situ tracer incubations and porewater sampling (Emerson et al. 1984). Solute exchange rates determined from benthic flux measurements and porewater profiles of tracers require the knowledge of tracer reaction rates or the assumption of an unreactive tracer, the relative permeability of burrow walls and linings to different solutes, and relative solute exchange rates in the presence of irrigation. Both naturally occurring (e.g.,  $^{222}\text{Rn}/^{226}\text{Ra}$  disequilibrium: Berelson et al. 1982, 1987, 1998; Hammond et al. 1977; Martin and Banta 1992; and references therein) and artificial (e.g., NaBr: Martin and Banta 1992; Sayles and Martin 1995;  $^2\text{H}$ : Berelson et al. 1999) tracers have been used to determine irrigation rates from comparisons and individual measurements of porewater profiles, benthic fluxes, sediment incubations, and water-column standing stocks. While useful, these techniques are subject to uncertainty related to the impacts of core retrieval and spatial variability because of the need to compare measurements obtained at adjacent locations or require SCUBA divers to conduct complex manipulations in situ.

Benthic chamber studies have calculated solute exchange across the SWI from chamber volume estimates and measured changes in chamber water solute concentrations over time (e.g., Jahnke and Jahnke 2000). A common technique used to

### Acknowledgments

We thank Carolyn D. Ruppel for assistance with early model development, and D. Hammond, C. Reimers, and W. Martin for helpful comments. We are also indebted to the officers and crew of the various early expeditions from which our dataset was taken. This study was supported by National Science Foundation (NSF) grants OCE99-11707 and OCE99-06897 to R. Jahnke. Time-series data were collected previously by R. Jahnke and supported by NSF.

**Table 1.** Sample sites and cruise designations

Location	Date, Ship (Cruise)	Deployment	ID	Depth (m)	Latitude	Longitude
Ceara Rise	March 1994 <i>R/V Knorr</i> (KN0394)	A1	CR1	3995	05°17.01'N	43°33.06'W
		B8	CR2	3272	05°15.09'N	44°08.16'W
		G40	CR3	4675	06°09.33'N	42°52.02'W
		G69	CR4	4677	06°09.40'N	42°52.25'W
Cape Verde plateau	November 1998 <i>R/V Knorr</i> (KN1198)	87	CV1	3103	18°27.86'N	21°01.48'W
		91	CV2	3102	18°28.01'N	21°01.54'W
Northern California margin	July 1992 <i>R/V New Horizon</i> (NH0792)	2	CA1	635	40°53.99'N	124°38.68'W
		33	CA2	720	40°05.16'N	124°27.95'W
		104	CA3	1330	40°50.64'N	124°46.111'W
		123	CA4	627	40°54.292'N	124°37.915'W
North Carolina slope depocenter	June 1993 <i>R/V New Horizon</i> (NH0693)	150	CA5	630	35°30.213'N	121°23.873'W
		7	NC1	850	36°05.02' N	74°44.11' W
		61	NC2	740	36°29.97' N	74°41.18' W
	July 1993 <i>R/V Cape Hatteras</i> (CH0793)	7	NC3	2927	32°42.27' N	75°50.98' W
		1	NC4	761	37°19.75'N	74°44.04'W
	September 1993 <i>R/V Cape Hatteras</i> (CH0993)	76	NC5	755	36°27.19'N	74°43.15'W
		116	NC6	855	35°23.08'N	74°49.76'W
	July 1994 <i>R/V Gyre</i> (GY0794)	117	NC7	2635	36°09.25'N	74°03.35'W
1		NC8	731	36°19.85'N	74°44.19'W	
August 1996 <i>R/V Edwin Link</i> (EL0896)		2	NC9	730	36°19.85'N	74°44.19'W
		3	NC10	607	35°50.73'N	74°49.32'W
		4	NC11	607	35°50.73'N	74°49.32'W
		5	NC12	742	35°25.04'N	74°48.37'W
	6	NC13	750	35°25.11'N	74°48.37'W	

estimate chamber volume is based on the initial dilution of a known amount of inert tracer (e.g., NaBr) injected into the chamber at the start of each incubation. Often the lack of a chamber water sample taken immediately upon tracer injection requires an indirect estimate of the initial chamber tracer concentration. This has been done with both linear and exponential extrapolations of tracer concentration time-series measurements (Jahnke and Jahnke 2000; Berelson et al. 1998). Because the chamber cross-sectional area is known, the chamber height can be derived from chamber volume. Each deployment must be evaluated individually to determine which extrapolation technique is most appropriate.

To examine further the uncertainties of the extrapolation to the initial tracer concentration, we apply a solute transport model similar to those used by Martin and Banta (1992), Sayles and Martin (1995), and Berelson et al. (1999) to estimate solute exchange rates and benthic chamber volume from benthic flux chamber tracer measurements. The measure-

ments used to test our model are from the U.S. mid-Atlantic slope depocenter (Jahnke and Jahnke 2000), the northern California margin (Jahnke unpubl. results unref.), the Ceara rise, and the Cape Verde plateau (Jahnke and Jahnke 2004).

### Procedures

**Dataset**—The specific study sites and cruises pertaining to the deployments that we modeled in this work are listed in Table 1. The benthic chamber instruments and analytical methods employed in these studies have been described in previous publications (e.g., Jahnke and Christiansen [1989] and Jahnke and Jahnke [2000]). Briefly, benthic chambers are deployed on the seafloor, either by submersible or by a free-vehicle benthic lander. The experiment begins upon closure of the chamber. NaBr tracer is injected into the flux chamber at the start of each incubation, and water samples are removed at preset times for tracer and nutrient analyses. Deployments on the EL0896 cruise (NC8 to NC13) were conducted with submersible-deployable benthic

**Table 2.** Bottom water and sediment characteristics at sample sites

ID	Bottom water O <sub>2</sub> (μM)	Benthic O <sub>2</sub> flux (mol m <sup>-2</sup> yr <sup>-1</sup> )	Carbon rain rate (mol m <sup>-2</sup> yr <sup>-1</sup> )*
CR1	263	-0.32	0.25
CR2	261	-0.19	0.15
CR3	232	-0.17	0.14
CR4	232	-0.22	0.17
CV1	242	-0.71	0.55
CV2	242	-1.24	0.95
CA1	25	-0.70	0.54
CA2	25	-0.82	0.63
CA3	33	-1.75	1.34
CA4	20	-0.95	0.73
CA5	15	-0.40	0.31
NC1	245	-1.58	1.22
NC2	245	-1.86	1.43
NC3	245	-0.52	0.40
NC4	245	-1.47	1.13
NC5	245	-3.35	2.57
NC6	245	-3.33	2.56
NC7	245	-0.61	0.47
NC8	245	-1.14	0.88
NC9	245	-2.82	2.17
NC10	245	-4.02	3.09
NC11	245	-3.69	2.83
NC12	245	-4.93	3.79
NC13	245	-3.43	2.64

\*Assumes 138:106 Redfield ratio

chambers, 30 cm in diameter (chamber area = 660.5 cm<sup>2</sup>). With the exception of CV2, all other deployments were conducted with a free-vehicle benthic chamber instrument containing 30 cm × 30 cm titanium chambers (chamber area = 893 cm<sup>2</sup>). The latter includes a scoop that captures the sediment contained within the chamber walls at the end of the experiment. Deployment CV2 was conducted with a free-vehicle instrument containing a 30-cm-diameter PVC chamber. No scoop was included in this experiment to recover sediment.

Bottom water and sediment characteristics are listed in Table 2. Bottom water oxygen concentrations range from 15 μM on the northern California margin to 263 μM on the Ceara rise. O<sub>2</sub> flux measurements range from -0.19 mol m<sup>-2</sup> yr<sup>-1</sup> on the Ceara Rise to -4.93 mol m<sup>-2</sup> yr<sup>-1</sup> on the North Carolina slope. Carbon rain rates were calculated from benthic O<sub>2</sub> fluxes assuming Redfield stoichiometry. Note that deviations from the Redfield ratio and burial of reduced metabolites produced by anaerobic mineralization at organic-rich sites on the northern California margin and the North Carolina slope depocenter may result in a significant discrepancy between true carbon rain rates and those calculated from benthic O<sub>2</sub> fluxes. Benthic fluxes of oxygen, titration alkalinity, total inorganic carbon, excess bromide, and nutrients for deployments in the Ceara rise, Cape Verde plateau, and North Carolina

slope have been reported elsewhere (Jahnke and Jahnke 2000, 2004). Excess bromide is calculated as the measured bromide concentration corrected for background bromide in concurrent analyses of standard (International Association for Physical Sciences of the Ocean) seawater. We have estimated an uncertainty of 47 μM associated with our reported values of excess bromide, equal to the sample standard deviation of 2 to 4 repeated measurements of 61 different samples analyzed in our laboratory.

Benthic chamber silicate and bromide results are shown in Fig. 1 and 2. In the majority of datasets from the North Carolina slope, Ceara rise, northern California margin, and Cape Verde plateau, bromide concentrations decreased slowly with time during the incubation (Fig. 1). Silicate concentrations increased steadily during each of these deployments, due to the dissolution of biogenic silica in the sediments. Steeper declines in excess bromide and increases in silicate concentrations are evident in six datasets from the Ceara rise, California margin, and Cape Verde plateau (Fig. 2). Fig. 3 displays benthic chamber oxygen results for these six datasets. Silicate concentrations in deployments CA2, CA3, and CA4 stop rising after approximately 10, 20, and 32 h, respectively. Excess bromide concentrations in deployments CA2 and CA3 began to decline more rapidly 10 and 20 h after the beginning of the incubation (Fig. 2).

Measured excess bromide concentrations follow an apparent increasing trend in deployments NC3 and NC6, as well as in the beginning of deployment CA3 due to the high density of the 0.6 M NaBr solution used in deployments prior to 1996 (Fig. 1 and 2). We assume that upon injection of the tracer in these deployments, the denser NaBr solution sank to the bottom of the chamber. Over time, this layer was mixed throughout the chamber. The first excess bromide data points from datasets CA1 and CA3 were not considered in the simulation of tracer transport in these deployments, whereas the entire datasets from NC3 and NC6 were not modeled because slow mixing of the tracer completely masked the effect of solute exchange between the chamber and the porewater. In addition, we ignored the first excess bromide data point measured in deployment NC12. Although a less dense 0.3 M NaBr solution was used in this deployment, an anomalously low tracer concentration was measured in the first water sample.

*Model description and assumptions*—A one-dimensional, grid-centered finite difference model of benthic solute exchange in flux chambers was developed to simulate the change in chamber water excess bromide concentrations with time over the duration of each deployment. We assume that excess bromide acts as an inert tracer and does not react with the sediments or impact natural irrigation or bioturbation rates. No significant evidence was found for an effect of NaBr on sediment irrigation or respiration rates (Martin and Banta 1992). Whereas a small amount of bromide is associated with sedimentary organic carbon and therefore released during remineralization, the observed Br/C ratio in sedi-

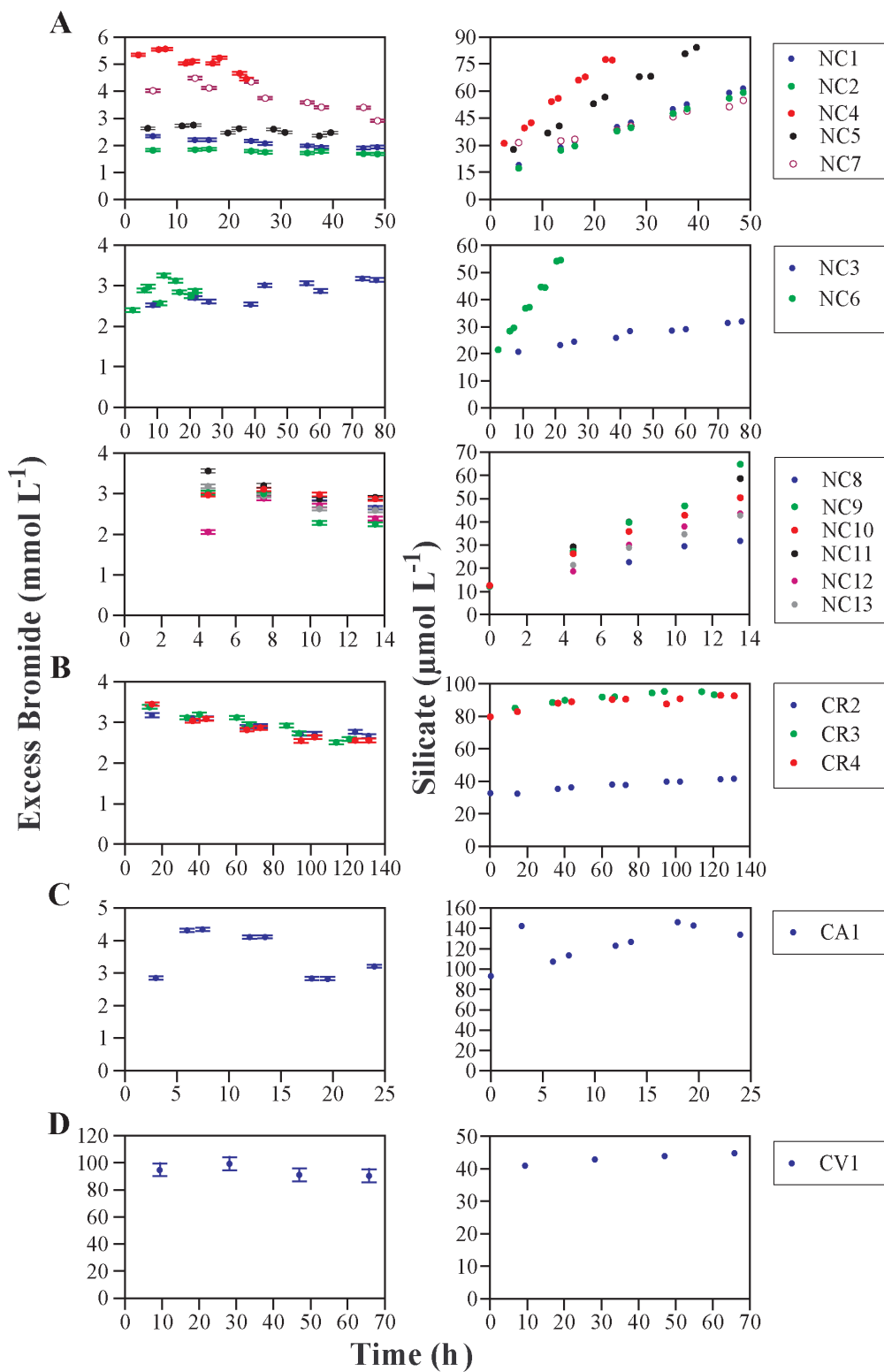


**Fig. 1.** Observed changes in chamber water excess bromide and silicate concentrations during benthic chamber deployments in the (A) North Carolina slope depocenter, (B) Ceara rise, (C) northern California margin, and (D) Cape Verde plateau. Analytical error in silicate measurements is small ( $\pm 1\%$ ); error bars for these data have been omitted because they are the size of the symbol.

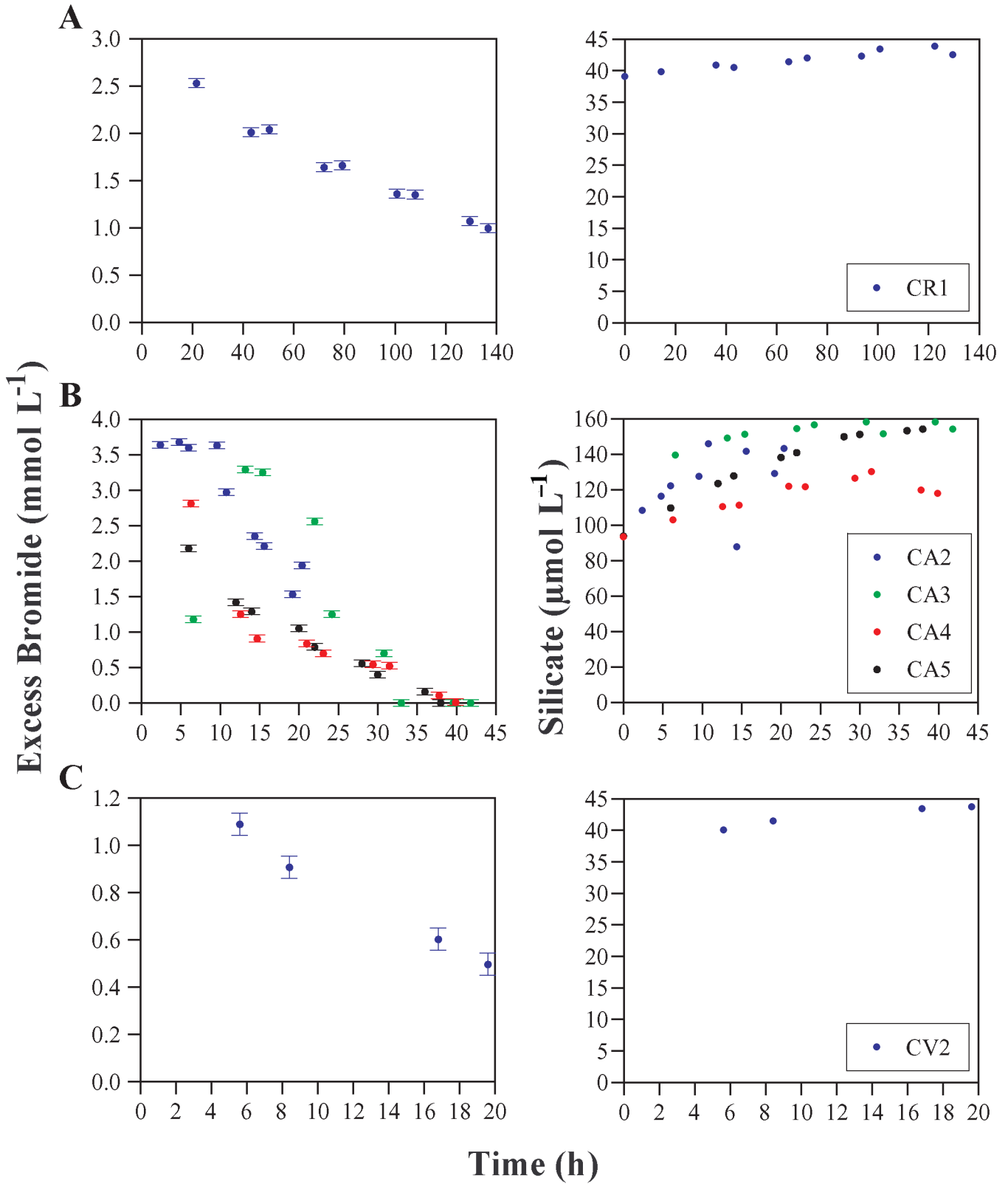


**Fig. 2.** Observed changes in chamber water excess bromide and silicate concentrations during benthic chamber deployments in the (A) Ceara rise, (B) northern California margin, and (C) Cape Verde plateau.

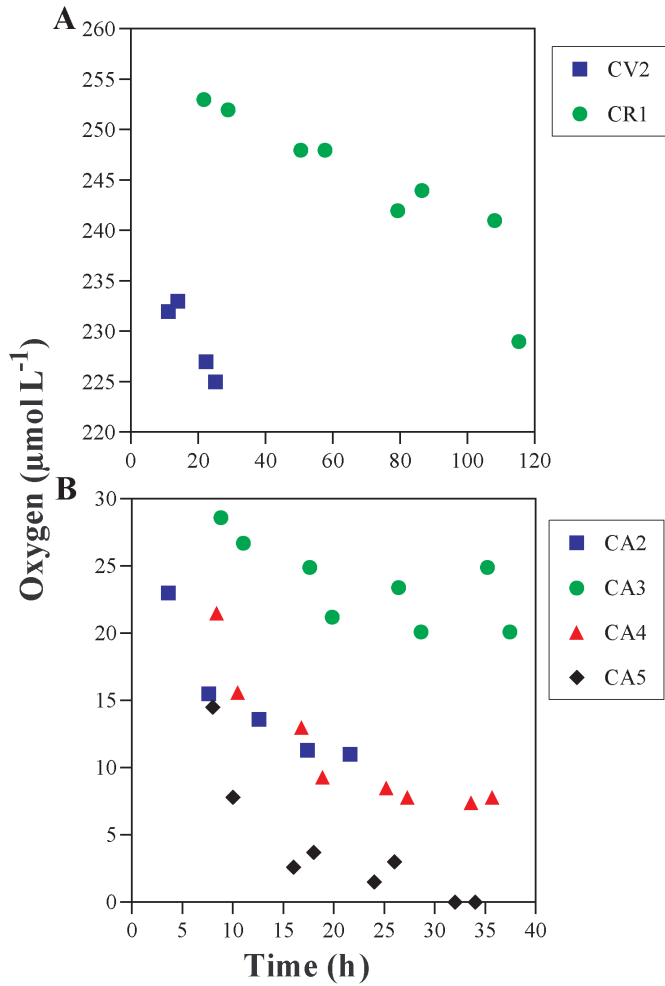


**Fig. 3.** Benthic chamber oxygen results for datasets with steep declines in chamber water excess bromide: (A) CR1, CV2, and (B) CA2, CA3, CA4, and CA5.

ments is on the order of  $2 \times 10^{-3}$  mol Br/mol C (Martin and Banta 1992). The resulting benthic bromide flux due to remineralization is negligible when compared to the amount of tracer injected. Further supporting these assumptions, previous authors have reported no significant adsorption of excess bromide onto marine sediments (Roychoudhury et al. 1998) or the organic linings of burrows of benthic macrofauna (Aller 1983).

The model includes two layers, representing the overlying water enclosed in the benthic chamber and porewater in the sediments below. We assume that the presence of a diffusive sublayer (DSL) overlying the sediment surface has a negligible impact on the exchange of tracer between the chamber and porewater. Calculations that support this assumption will be presented in the Assessment section. Each experiment is initiated at the time of tracer injection into the chamber, so that all of the tracer is mixed into the chamber water, but has not yet begun to exchange into the underlying porewater. Benthic

solute exchange occurs throughout the duration of each experiment by molecular diffusion and either biologically enhanced diffusion (bioturbation) or irrigation of macrofaunal burrows. Diffusive and nonlocal exchange (NLE) mechanisms are represented in Eq. 1,

$$\phi \frac{\partial C}{\partial t} = \epsilon D_0 \frac{\partial}{\partial z} \left( \frac{\phi}{\theta^2} \frac{\partial C}{\partial z} \right) + \alpha \phi (C_0 - C) \quad (1)$$

where  $D_0$  is the diffusion coefficient for bromide in seawater ( $\text{L}^2 \text{T}^{-1}$ ),  $\phi$  is the dimensionless sediment porosity,  $\theta$  is the dimensionless sediment tortuosity,  $C$  is the tracer concentration ( $\text{M L}^{-3}$ ),  $t$  is time (T),  $z$  is the distance (L) below the SWI,  $M$  is mass, and  $\epsilon$  is the dimensionless diffusion enhancement factor, which is set to values larger than one to increase the apparent value of the diffusion coefficient due to biodiffusion. The porosity profile is assumed to be at steady state but is allowed to vary with depth, as described below.

The second term on the right-hand side of Eq. 1 represents NLE, where  $C_0$  is the concentration of tracer in the chamber and  $C$  represents the concentration of tracer in the porewater at each depth interval of the vertical domain. The term  $\alpha$  ( $\text{T}^{-1}$ ) represents the exchange rate of a solute between bottom water and porewater due to molecular diffusion across burrow walls, assuming the solute concentration inside the burrow is equal to that in the overlying water, due to flushing by macrofauna (Boudreau 1984, 1997).

A central difference formula was applied with a vertical spatial domain of 2 m, a time step of 0.001 h, and 1-mm depth resolution. In the model, both the chamber water and the porewater within every 1-mm interval of the modeled sediment domain are instantaneously mixed at each time step, so that the distribution of tracer is always homogeneous in the chamber and in the sediment intervals. At  $t = 0$ ,

$$\text{excess } [\text{Br}]_{\text{chamber}} = \text{moles of excess bromide injected/chamber volume}, \quad (2)$$

$$\text{and excess } [\text{Br}]_{z > 0} = 0. \quad (3)$$

Excess bromide in the chamber water is recalculated at each time step. Mass balance requires that the change with time in the amount of excess bromide in the overlying chamber water is equal to the flux across the SWI. At  $z = 0$ ,

$$\text{excess } [\text{Br}]_{z=0} = \text{excess } [\text{Br}]_{\text{chamber}} \quad (4)$$

A Neumann (no flux) boundary condition is applied at the bottom boundary.

*Constant model inputs*— $D_0$  was calculated according to temperature- and salinity-dependent relationships supplied by Boudreau (1997), on the basis of work by Li and Gregory (1974). For all model runs, porosity is calculated from Eq. 5, decreasing from 0.868 at the SWI to 0.712 at depth (Martin and Sayles 1996):

$$\phi(z) = 0.712 + 0.156 \times e^{-0.512z} \quad (5)$$

This profile approximates measured profiles from a variety of deep-sea locations (Reimers 1987; Hammond et al. 1996). Tortuosity is estimated from Archie's Law,  $\theta^2 = \phi^{1-m}$ , with  $m = 3$  for fine-grained sediments such as those discussed in this paper.

*The infinite NLE case*—An “infinite” NLE (infNLE) model was applied to those datasets in which chamber tracer concentrations declined below levels achievable by enhanced diffusion and NLE. In this model, the value of  $C$  in the NLE term of Eq. 1 is set to zero. This model simulates the decline of chamber tracer concentrations due to exchange of chamber water and surrounding bottom water through the irrigation of connecting worm burrows. The amount of tracer in the volume of chamber water exchanged by this mechanism is, therefore, permanently removed from the model domain at each time step and is not added to the porewater in the vertical sediment section simulated by the model. Therefore, there is no depth-dependence associated with  $\alpha$  in this model. However, for the purposes of consistency and comparison with other model results, we have chosen to apply the infNLE model in 100 increments representing the top 10 cm of the vertical spatial domain. Using this parameterization, it is possible to make comparisons between  $\alpha$  values associated with models including NLE to 10 cm and infNLE.

*Depth-dependence of nondiffusive exchange*—The depth over which bioirrigation and biodiffusion dominate solute and particle mixing varies from location to location. For example, in the Panama Basin, rapid mixing dominates the upper 6 to 8 cm of sediment, whereas slower mixing may persist to >30-cm depth (Aller 1990 and references therein). In contrast, Schlüter et al. (2000) considered NLE in depth intervals from 0 to 2.5 cm, 2.5 to 5 cm, and 5 to 10 cm. To test the sensitivity of our derived chamber volume and exchange parameters, we have compared models with enhanced diffusion to 5, 10, and 20 cm and NLE to 5, 10, and 20 cm. We have also compared a model of NLE to 1.5 m with the infNLE model. The results of these simulations are shown in the Discussion section.

## Assessment

*Model characteristics and sensitivity*—Previous calibration studies estimated the thickness of the DSL within our chambers to be 300  $\mu\text{m}$  to 500  $\mu\text{m}$  (Buchholtz-ten Brink et al. 1989) at the stirring rate employed. To verify our assumption that the exclusion of a diffusive sublayer would not affect our model results significantly, model runs were performed with DSL thicknesses of 0, 300, and 500  $\mu\text{m}$ , assuming that molecular diffusion dominated solute exchange (Fig. 4). Note that the distinct steps that are evident in the plots of simulated excess  $[\text{Br}^-]$  represent the dilution of chamber water excess  $[\text{Br}^-]$  with surrounding bottom water due to the removal of each time-series sample. These results are consistent with the model of Reimers et al. (2001), which was used to show that halving or doubling the diffusive sublayer thickness in a

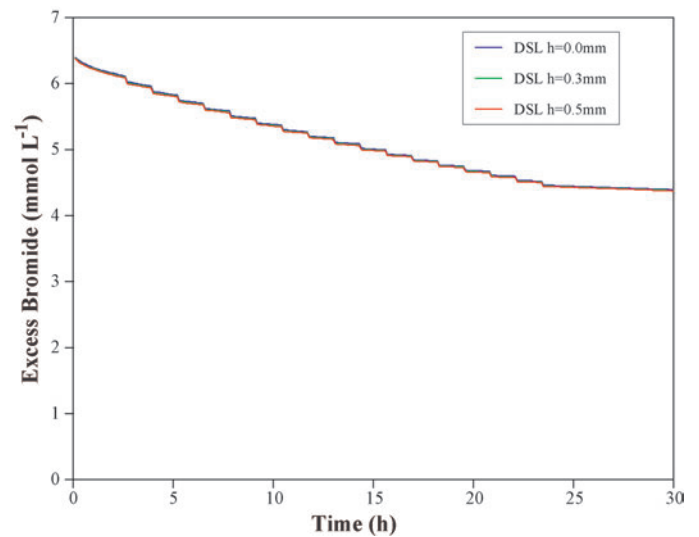


**Fig. 4.** The effect of diffusive sublayer thickness on model results—deployment NC4.

model incubation longer than 10 to 20 h has a negligible effect on model outputs of benthic oxygen fluxes. Sublayer thickness exerts little influence on excess bromide flux across the SWI because the slow changes in the excess bromide concentration difference across the DSL imply that the accumulation rate of bromide in the porewater is the limiting factor (Archer et al. 1989).

Tracer datasets were simulated by selecting values of the unknown model parameters for enhanced diffusion, NLE, and chamber volume that best reproduce the measured changes in chamber water tracer concentrations. Fig. 5 illustrates the sensitivity of the model to changes in each variable. Changes in chamber volume primarily cause vertical displacement (Fig. 5A, 5C, 5E, and 5G), while increasing the values of  $\epsilon$ ,  $\alpha$ , and the penetration of NLE generates more curvature in the plots, such that chamber water tracer concentrations decline more rapidly at the beginning of the incubation (Fig. 5B, 5D, 5F, and 5H). The potential draw-down of tracer is determined by the volume of porewater into which exchange occurs. If solute exchange is controlled by molecular diffusion, in 22 h the mean penetration depth of the tracer into the sediments is approximately 0.9 cm. In this case (Fig. 5B;  $\epsilon = 1$ ), the chamber water tracer concentration decreases only slightly. If NLE is limited to this same thin layer of sediment, a similar decrease is observed (Fig. 5D). As the effective rate of diffusive exchange is increased, the mean penetration depth of tracer into the sediment increases and chamber water tracer concentrations decrease further. After an incubation of 22 hours at  $\epsilon = 120$ , the mean penetration depth of the tracer is approximately 10 cm, and lower concentrations of tracer are observed in the chamber (Fig. 5B). Similarly, lower tracer concentrations are estimated at all but the smallest value of  $\alpha$  if the zone of NLE is expanded 0 to 10 cm (Fig. 5F). Note the nearly constant tracer concentrations achieved after a few hours of incubation

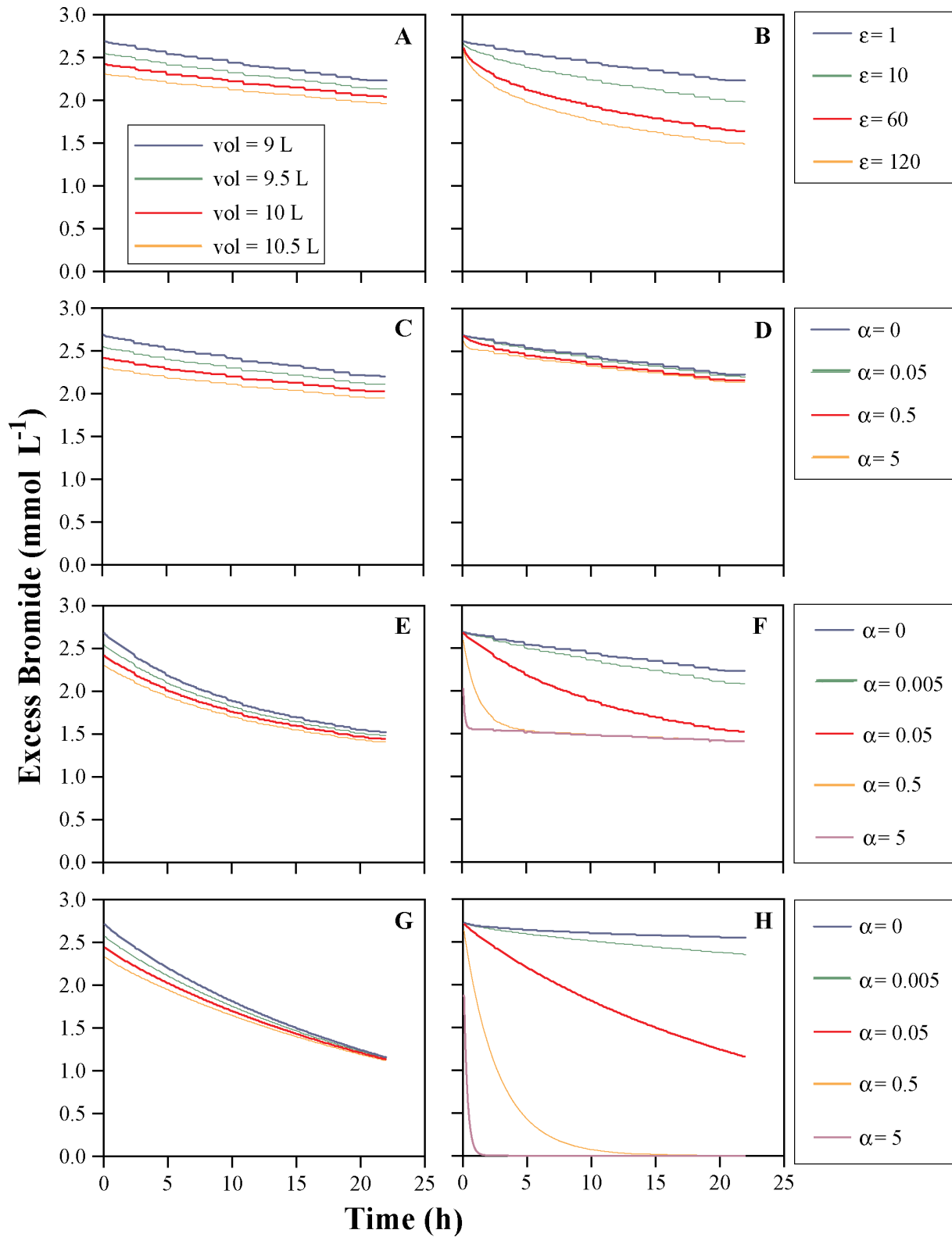


**Fig. 5.** Sensitivity of tracer transport simulation to model parameterization: (A) varying chamber volume at  $\epsilon = 1$  with no NLE; (B) varying  $\epsilon$  at chamber volume = 9 L with no NLE; (C) varying chamber volume at constant NLE to 0.9 cm sediment depth,  $\alpha = 0.05$  and  $\epsilon = 1$ ; (D) varying NLE to 0.9 cm sediment depth at chamber volume = 9 L and  $\epsilon = 1$ ; (E) varying chamber volume at constant NLE to 10 cm sediment depth,  $\alpha = 0.05$  and  $\epsilon = 1$ ; (F) varying NLE to 10 cm sediment depth at chamber volume = 9 L and  $\epsilon = 1$ ; (G) varying chamber volume at constant NLE to 10 cm sediment depth,  $\alpha = 0.05$ ,  $\epsilon = 1$ , using infNLE model; (H) varying NLE to 10 cm sediment depth at chamber volume = 9 L,  $\epsilon = 1$ , using infNLE model.

with high rates of NLE (Fig. 5F). In these cases, nonlocal solute exchange has homogenized the distribution of tracer throughout the irrigated zone and chamber. The slow decline of chamber water tracer concentrations beyond this point in these simulated incubations is due to molecular diffusive solute exchange rates below the irrigated layer. Tracer concentrations near zero can only be achieved if the tracer is exchanged with a much larger volume, as simulated by the infNLE model detailed in the *Model description and assumptions* section (Fig. 5H).

Reduced chi-squared analyses were used to determine best-fit scenarios for each dataset. Best-fit model parameters and their respective reduced  $\chi^2$  values are shown in Tables 3, 4, and 5.

*Solute exchange by molecular diffusion*—As shown in Table 3, best-fit simulations were obtained for six tracer datasets from deployments on the Ceara rise, the Cape Verde plateau, and the North Carolina slope depocenter with solute exchange rates equal to molecular diffusion (MD;  $\epsilon = 1$ ). For each simulation, the vertical position of the curve was adjusted to match the dataset by selecting the value of chamber volume that produces the lowest  $\chi^2$ . Best-fit model simulations and the results of changing chamber volume by  $\pm 0.1$  to 0.2 L from best-fit values are displayed for comparison in Fig. 6 and Table 3. Extrapolation to  $t = 0$  with a linear regression is also included. Except for deployment CV1, the estimates of chamber volume based on linear extrapolation of these datasets are larger than the values obtained from our best-fit model results, although the average difference is only 5.6%.

*Solute exchange by enhanced diffusion*—Best-fit simulations were obtained with enhanced diffusive exchange rates of 2 – 78  $\times$  MD for 10 tracer datasets from the Ceara Rise, North Carolina slope depocenter, and Northern California margin (Fig. 7, Table 3). Additional model runs with enhanced diffusion coefficients surrounding the best-fit values are included in Fig. 7 and Table 3 to demonstrate parameter sensitivity. Chamber volume estimates for these additional model runs are best-fit values for each  $\epsilon$ , although in every case,  $\chi^2$  statistics for these models are higher than for the overall best-fit model.

Several model runs were carried out to test the depth-dependence of  $\epsilon$ . As is evident from the results shown in Table 4, models with enhanced diffusion to 10 cm and 20 cm are indistinguishable in every case. Results with enhanced diffusion to 10 cm and 5 cm are also almost indistinguishable, except in the case of the two deployments with the highest  $\epsilon$  values—NC9 and NC12—where  $\chi^2$  is significantly higher for models run with enhanced diffusion to 5 cm. It is apparent from these results that this model cannot be used to determine the depth dependence of biodiffusion, but also that the chamber volume and net exchange rate estimates are robust and not highly sensitive to variations in the vertical spatial extent of solute exchange, at least in the range of 5 to 20 cm.

The estimates of chamber volume based on linear extrapolation of all 10 datasets modeled with enhanced diffusive

**Table 3.** Summary of in situ benthic flux model results for datasets modeled with molecular and enhanced diffusion only\*

ID	Simulated chamber		
	volume (L)	$\epsilon$	$\chi^2$
CA1	5.75	1	19.41†
	4.75	11	8.63†
	4.25	21	11.04†
CV1	13.80	1	0.16†
	14.00	1	0.03†
	14.20	1	0.11†
NC1	11.25	1	2.83
	10.00	9	0.60
	9.40	17	1.33
NC2	13.6	1	0.90
	13.8	1	0.55
	14.0	1	0.85
NC4	3.80	1	56.78
	3.90	1	47.47
	4.00	1	51.38
NC5	9.50	1	5.88
	9.70	1	4.29
	9.90	1	5.43
NC7	4.80	1	50.90
	4.90	1	49.69
	5.00	1	53.13
NC8	3.30	14	2.04
	2.95	24	0.61
	2.65	34	1.21
NC9	2.85	58	26.93
	2.50	78	25.78
	2.20	98	27.65
NC10	4.00	1	0.56†
	3.90	2	0.09†
	3.80	3	0.18†
NC11	3.15	13	7.36
	2.95	18	6.68
	2.80	23	7.25
NC12	3.15	30	2.85†
	2.65	50	1.66†
	2.20	70	2.19†
NC13	3.55	14	3.33
	3.30	22	2.25
	3.10	30	2.88
CR2	7.00	1	4.11
	7.15	1	2.2
	7.30	1	3.28
CR3	6.80	1	5.48
	6.40	2	4.75
	6.15	3	5.92
CR4	6.85	1	5.91
	6.15	3	2.54
	5.65	5	4.89

\*The reduced  $\chi^2$  statistic is calculated with 2 degrees of freedom, representing  $\epsilon$  and chamber volume.

† $\chi^2$  for calculation excluding flyer data points.

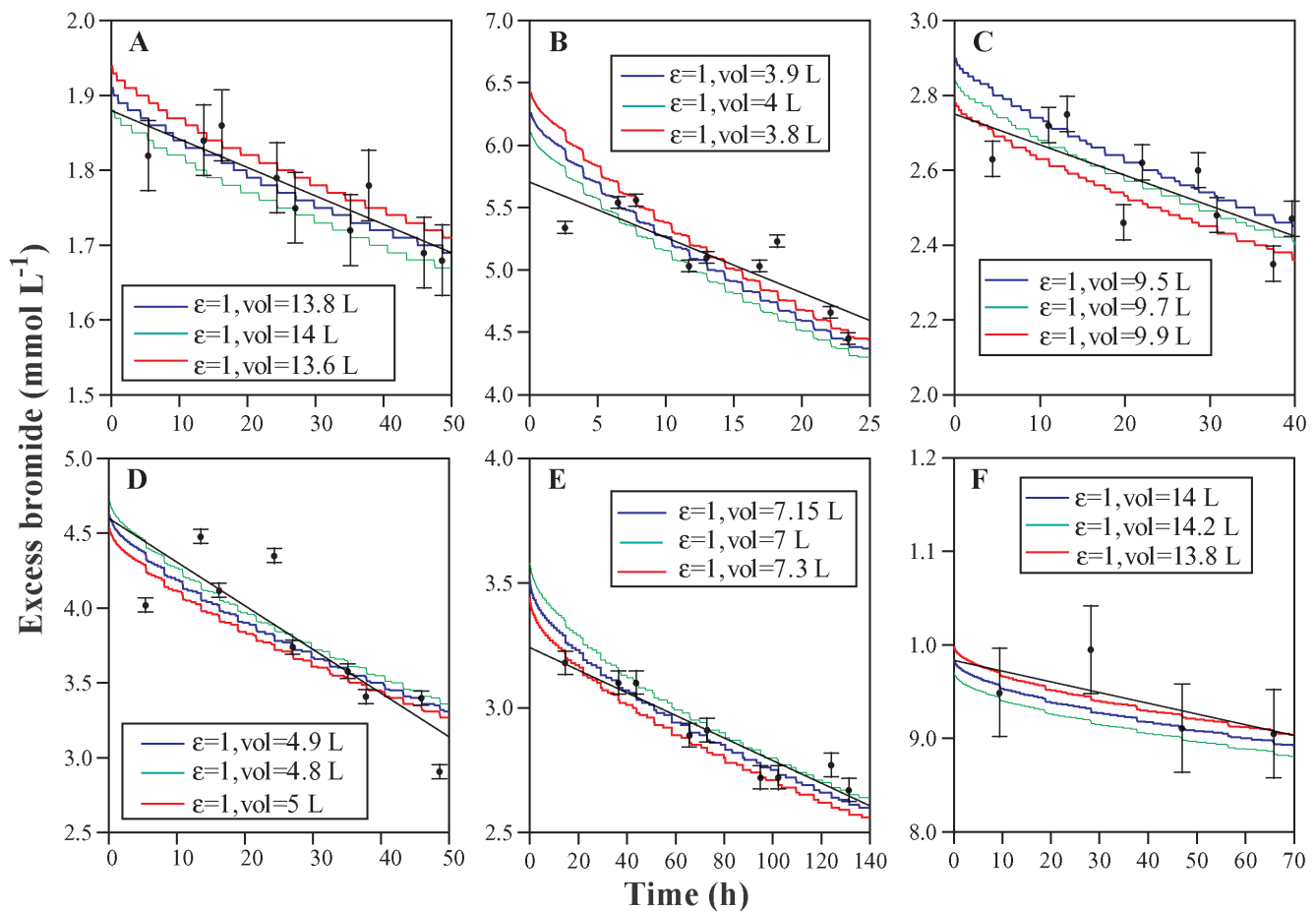


**Fig. 6.** Tracer datasets and model simulations for deployments (A) NC2, (B) NC4, (C) NC5, (D) NC7, (E) CR2, and (F) CV1. Solid black line represents linear regression; filled circles represent data.

exchange are larger than the values obtained from our best-fit model results, with an average difference of 20.5%.

*Nonlocal solute exchange*—Tracer datasets CR1, CV2, CA2, CA3, CA4, and CA5 were simulated with NLE. Best-fit parameter values are listed in Table 5.

If NLE occurs only inside the model domain over the top 10 cm of sediment, the minimum achievable chamber water tracer concentration is approximately 32% of the initial value, given efficient exchange of tracer across burrow walls, resulting in a homogeneous distribution throughout the chamber water and the top 10 cm of sediment. This calculation assumes a uniform porosity of 0.868—the maximum value at the surface of the modeled sediment section—and a minimum chamber height of 4 cm, although it neglects the small effect of molecular diffusion below the irrigated surface sediment layer. Even so, this scenario cannot explain a decline in chamber water tracer concentrations to the undetectable levels observed at the end of the deployments CA3, CA4, and CA5. Therefore, solute exchange for these deployments was simulated with the infNLE model explained in the *Model description and assumptions* section.

The large dilution of tracer (0.4% and 0.3% of injected concentrations) observed already in the excess [Br<sup>-</sup>] measured in the first chamber water samples of deployments CR1 and CV2 require larger chamber heights, on the order of 10 cm. At these sites, the minimum achievable chamber water tracer concentration is approximately 54% of the initial value, given NLE to 10 cm sediment depth, and assuming a chamber height of 10 cm and a homogeneous porosity distribution of 0.868. Because this effect is too small to account for the degree of tracer exchange observed in the chamber water during these deployments, we applied the infNLE model to simulate these two datasets, as well.

Best-fit simulations obtained for CA2 with NLE, and for CA4, CA5, CA3, CV2, and CR1 with infNLE were obtained by optimizing values of  $\alpha$  and chamber volume in each of these models (Fig. 8). The abrupt changes in temporal trends of decreasing chamber water excess [Br<sup>-</sup>] observed during deployments CA2 and CA3 suggest corresponding changes in solute exchange rates, perhaps due to the response of benthic macrofauna to declining dissolved oxygen concentrations in chamber water, as will be discussed below. Additional results from

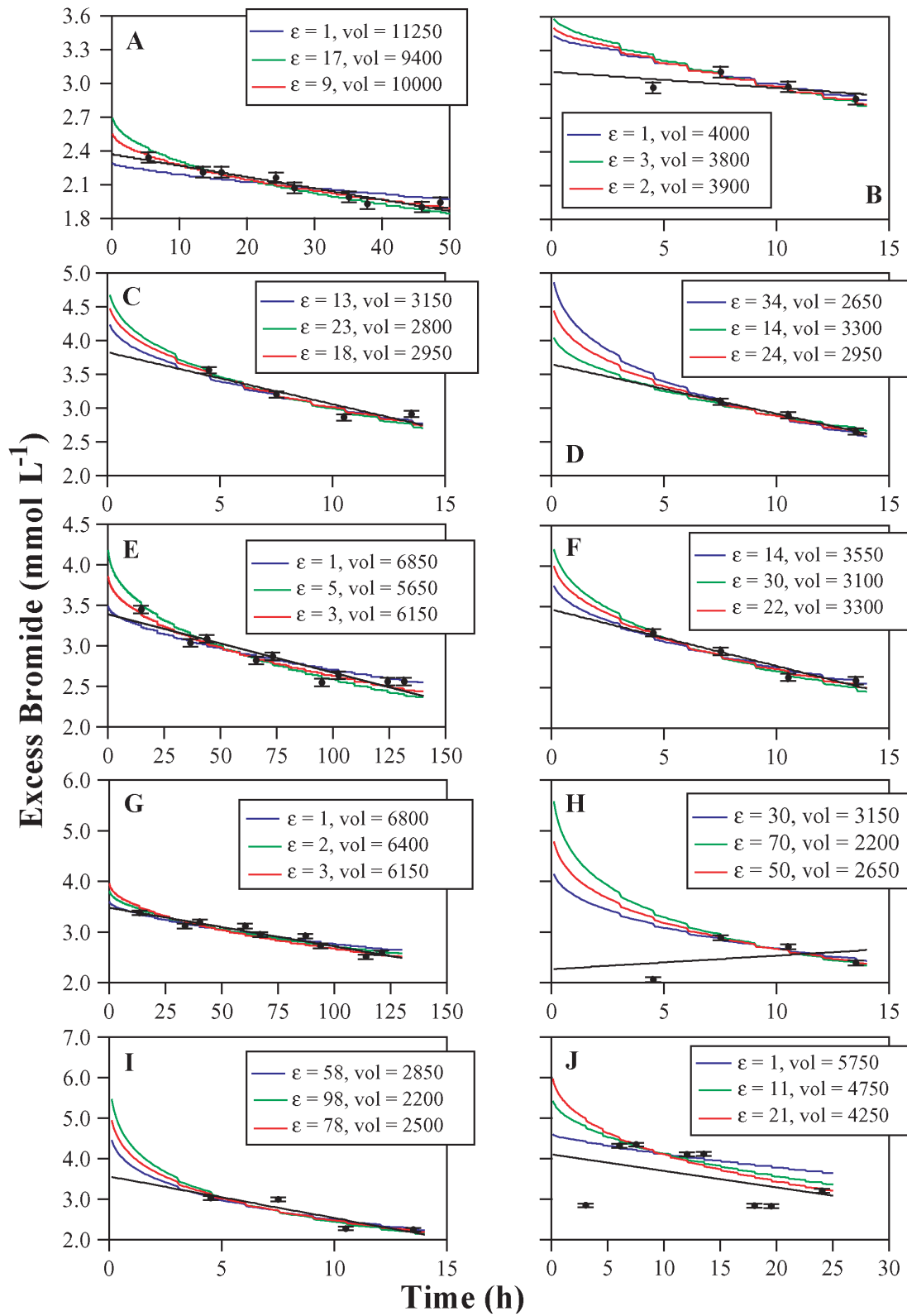


**Fig. 7.** Tracer datasets and simulations for deployments modeled with enhanced diffusion. (A) NC1, (B) NC10, (C) NC11, (D) NC8, (E) CR4, (F) NC13, (G) CR3, (H) NC12, (I) NC9, (J) CA1. Solid black line represents linear regression; filled circles represent data.

**Table 4.** Summary of depth-dependence of enhanced diffusion model results\*

ID	$\epsilon_{1-20}$	$V_{1-20}$ (L)	$\chi^2_{1-20}$	$\epsilon_{1-10}$	$V_{1-10}$ (L)	$\chi^2_{1-10}$	$\epsilon_{1-5}$	$V_{1-5}$ (L)	$\chi^2_{1-5}$
CA1	11	4.75	8.63	11	4.75	8.63	11	4.75	8.69
NC1	9	10.00	0.60	9	10.00	0.60	9	10.00	0.61
NC8	24	2.95	0.61	24	2.95	0.61	24	2.95	0.67
NC9	78	2.50	25.78	78	2.50	25.78	45	3.10	34.03
NC10	2	3.90	0.09	2	3.90	0.09	2	3.90	0.09
NC11	18	2.95	6.68	18	2.95	6.68	18	2.95	6.58
NC12	50	2.65	1.66†	50	2.65	1.66†	37	3.00	3.08†
NC13	22	3.3	2.25	22	3.3	2.25	22	3.3	2.25
CR3	2	6.40	4.75	2	6.40	4.75	2	6.45	4.76
CR4	3	6.15	2.54	3	6.15	2.54	3	6.15	2.50

\*The reduced  $\chi^2$  statistic is calculated with 2 degrees of freedom, representing  $\epsilon$  and chamber volume.

† $\chi^2$  for calculation excluding flyer data points.

models with  $\alpha$  values bracketing the best-fit value are also included for comparison in Table 5 and Fig. 8. Values of chamber volume for all additional model runs were selected to yield the lowest  $\chi^2$ . Except for CA2, the estimates of chamber volume based on linear extrapolation of all six datasets modeled with NLE are larger than the values obtained from our best-fit model results, with an average difference of 21%.

Leslie et al. (1990) found evidence of macrofaunal irrigation to approximately 1.5 and 2.0 m in the Santa Catalina and San Nicolas basins, respectively, in the California borderland. It is likely that such deep burrow networks would extend diagonally into the sediment, and out of the spatial domain included in the model, as simulated in the infNLE case. However, it is important to note that irrigation to 1.5-m sediment depth simulated with the NLE model could also explain the exceptionally large decline in chamber tracer concentrations of the five datasets simulated with the infNLE model (Fig. 8B through 8F; Table 5). The same calculation applied above can be used to show that the minimum achievable chamber water tracer concentration is approximately 3% of the initial value, assuming NLE to 1.5-m sediment depth. Although this scenario can explain significant solute exchange rates, it cannot explain the undetectable concentrations of tracer measured at the end of deployments CA3, CA4, and CA5. While it is probable that burrows to 1.5 m exist at the sites of the five deployments simulated with infNLE, it is unlikely that the distribution of deep burrows within the sediment area enclosed in these chamber deployments is dense enough to explain the intense irrigation required to achieve homogeneous tracer distributions to 1.5 m within the duration of one deployment.

In deployments CA2 and CA3, chamber water tracer concentrations declined slowly for the first 10 and 20 h, after which they began to decrease rapidly. Silicate concentrations rose steadily for the first period, then leveled off (Fig. 2B). These trends suggest that whereas both incubations were closed to

**Table 5.** Summary of in situ benthic flux model results for datasets modeled with nonlocal exchange\*

ID	Model	Simulated chamber volume (L)		
		volume (L)	$\alpha$	$\chi^2$
CA2	NLE to 10 cm (>9.65 hrs)	6.35	0.100	17.87
		6.30	0.125	15.38
		6.25	0.150	17.19
CA3	NLE to 5 cm NLE to 20 cm infNLE to 10 cm (>21 hrs)	6.30	0.520	54.46
		6.30	0.041	15.57
		7.55	0.250	19.79†
CA4	infNLE to 10 cm	7.55	0.275	18.11†
		7.50	0.300	19.17†
		7.50	0.023	28.88†
CA5	NLE to 1.5 m infNLE to 10 cm	5.20	0.065	33.60
		5.35	0.072	24.39
		5.65	0.080	31.50
CV2	NLE to 1.5 m infNLE to 10 cm	3.90	0.0052	20.06
		8.10	0.065	29.25
		8.00	0.078	10.51
CR1	NLE to 1.5 m infNLE	8.20	0.085	14.98
		7.10	0.0058	21.04
		9.60	0.095	1.26
CR4	infNLE to 10 cm	9.25	0.101	0.33
		8.95	0.107	1.17
		8.80	0.0078	0.31
CR3	NLE to 1.5 m	8.70	0.0085	3.59
		8.35	0.0092	1.94
		8.05	0.0099	3.95
CR4	NLE to 1.5 m	8.10	0.00067	2.24

\*The reduced  $\chi^2$  statistic is calculated with 3 degrees of freedom, representing  $\epsilon$ ,  $\alpha$ , and chamber volume.

† $\chi^2$  for calculation excluding flyer data points.

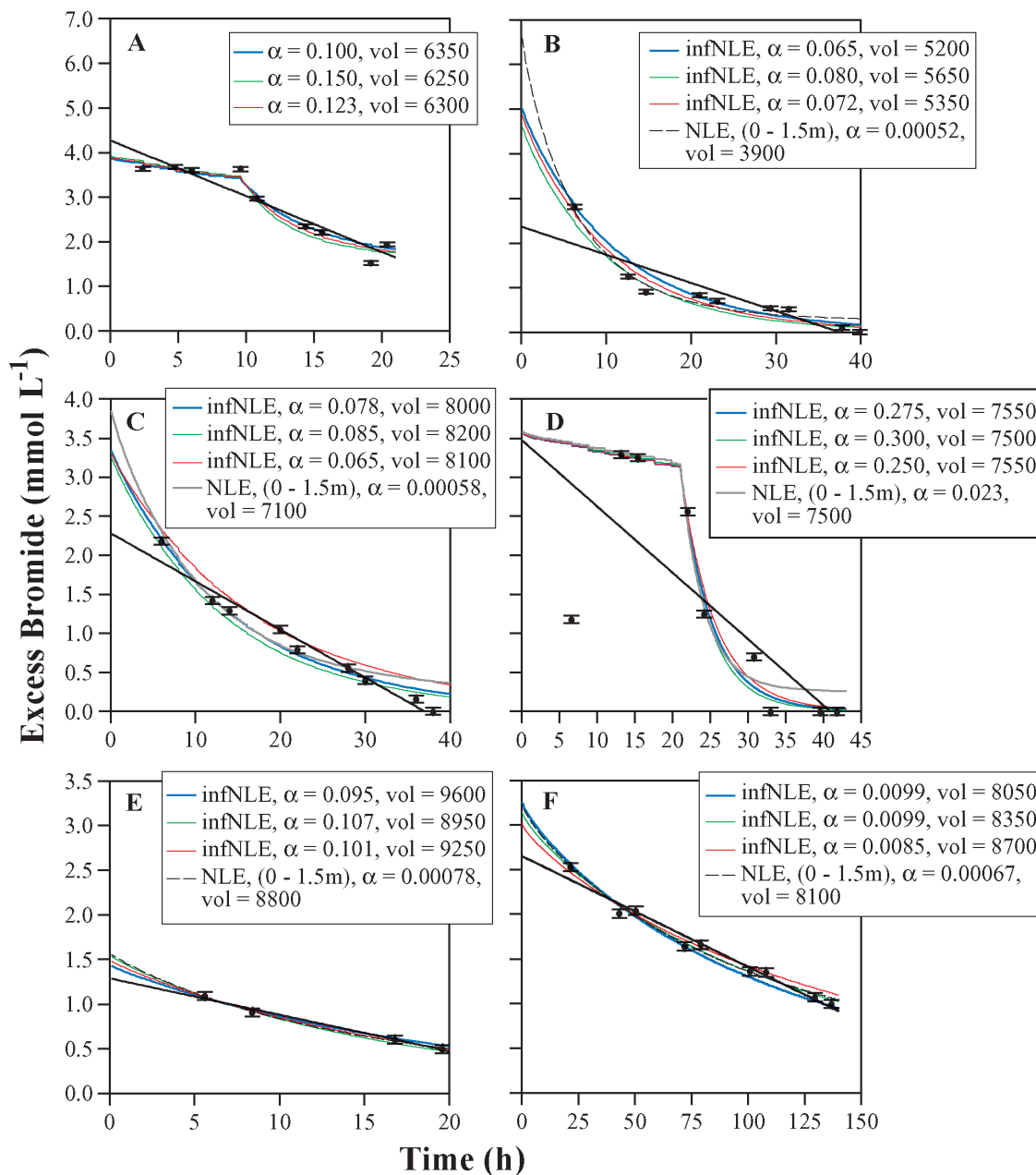


**Fig. 8.** Tracer datasets and simulations for deployments modeled with nonlocal exchange. (A) CA2, (B) CA4, (C) CA5, (D) CA3, (E) CV2, (F) CR1. Solid black line represents linear regression; filled circles represent data.

the surrounding bottom water, the apparent silicate concentrations of the rapidly exchanged porewater in these and all other deployments in this region were less than 200  $\mu\text{M}$ . Porewater silicate concentrations in the California margin near this site range from 400 to 700  $\mu\text{M}$  (Jahnke unpubl. data unref.), suggesting that the rapidly exchanged porewater has been diluted with bottom water, which is connected to the chamber water through burrows. Bioirrigation began 10 and 20 h after the beginning of the incubations, perhaps because of the response of benthic macrofauna to the low  $\text{O}_2$  concen-

trations that develop in chamber waters after several hours of  $\text{O}_2$  consumption by aerobic organic matter remineralization (Fig. 3). As a result, accelerated dilution of chamber water excess bromide was observed only after an initial period of solute exchange by molecular diffusion only. We simulated these trends by introducing nonzero values of  $\alpha$  approximately 10 and 20 h after the beginning of the model runs.

For deployment CA2, model results with NLE to 5, 10, and 20 cm are included in Table 5 for comparison. The 10-cm model is significantly better than the 5-cm model, but com-

parable to the 20-cm model. From these results, it is unclear whether or not the NLE model can be used to determine the depth-dependence of NLE.

Increasing silicate concentrations in the six deployments simulated with the NLE and infNLE models indicate that these incubations were closed to the surrounding bottom water. However, it is necessary to consider the possibility that significant exchange between chamber water and bottom water due to incomplete emplacement of a benthic chamber on the seafloor or a small leak might cause the rapidly declining chamber tracer concentrations observed in the six deployments simulated with NLE. This explanation is especially persuasive in view of the undetectable tracer concentrations measured at the end of deployments CA3 and CA5. In this scenario, increasing chamber silicate concentrations imply that the exchange of silicate across the SWI was balanced by a small leak, which at steady state would result in a constant chamber silicate concentration, higher than surrounding bottom water but lower than predicted by a closed incubation and exchange with high concentrations of porewater silicate.

Two lines of evidence suggest that the rapid tracer loss observed in deployments CA2, CA3, CA4, CA5, and CR1 is not due to a direct leakage between chamber and bottom waters. Because the chamber instrument used in these deployments recovers the chamber sediments, the seal between the chamber and the seafloor can be directly verified. For these deployments, a minimum of 10 to 15 cm of sediment was recovered, indicating that there was no channel for leakage around the bottom of the chamber. Visual examination of the lid upon recovery of the instrument also verified that the chamber top was sealed. A hydraulically driven closing mechanism that locks in place under significant force is employed. Also, it should be noted that large (approximately 5-cm diameter) burrows were observed, extending throughout the chamber sediments recovered at the northern California margin sites. Thus, high rates of irrigation are to be expected here. It is especially difficult to invoke chamber leaks to explain the rapid tracer losses observed in deployments CA2 and CA3. In these two cases, the required leaks would have to develop 10 and 20 h after the beginning of each deployment, because of the changing solute exchange rates observed in these datasets. In addition, the hypothetical leaks would have to be sealed before chamber recovery, because visual examination of chamber lids and recovered sediments were consistent with closed incubations. In view of this unlikely series of events, enhanced porewater exchange is the most evident explanation for the observed trends. Deployment CV2 was conducted with a modified free-vehicle benthic chamber instrument, without the ability to recover enclosed sediments. However, the best-fit chamber volume required to simulate the chamber water excess  $[Br^-]$  measured in this deployment suggests that the chamber enclosed approximately 15 cm of sediment.

We also have assessed the possibility of a leak by estimating the silicate flux that would be required to obtain the measured

silicate results if a chamber leak were responsible for the decrease in chamber water tracer concentrations. A leak rate can be approximated from the initial rate of change in chamber excess  $[Br^-]$ , the chamber volume estimated by our best-fit model, and the initial chamber excess  $[Br^-]$ . For CR1, CV2, CA4, and CA5 the initial rate of change in chamber excess  $[Br^-]$  was calculated from the first two data points; the initial chamber excess  $[Br^-]$  was taken from the first data point. For CA2 and CA3, the initial rate of change in chamber excess  $[Br^-]$  was calculated from the two data points following the abrupt trend changes at approximately 10 and 20 h during the incubation, whereas the initial chamber excess  $[Br^-]$  was taken from data points at approximately 10 and 20 h, respectively. The actual benthic silicate flux that would be required to explain the measured silicate results in the presence of this leak was determined from the calculated leak rate, the estimated chamber volume, bottom water silicate measurements, and the measured silicate flux. The first two chamber water silicate measurements were used for consistency in silicate flux and bromide leak rate. The calculated silicate fluxes are 11.74, 9.80, 1.05, 1.84, 0.04, and 0.51 mol Si m<sup>-2</sup> yr<sup>-1</sup> for CA2, CA3, CA4, CA5, CR1, and CV2, respectively. In comparison, 0.149 to 1.933 mol Si m<sup>-2</sup> yr<sup>-1</sup>, 0.031 to 0.058 mol Si m<sup>-2</sup> yr<sup>-1</sup>, and 0.083 to 0.345 mol Si m<sup>-2</sup> yr<sup>-1</sup> have been found for the North Carolina slope depocenter, Ceara rise, and Cape Verde plateau, respectively (Jahnke and Jahnke 2000, 2004). The calculated fluxes that would be required if the tracer loss was caused by a leak are greater than those reported previously for these types of environments, especially for deployments on the northern California margin. Taken together with the visual evidence, it appears that enhanced porewater exchange and not chamber leakage is the most probable explanation for these results.

*Comparisons: regional trends*—The Cape Verde plateau and the North Carolina slope depocenter have high organic carbon rain rates and high bottom water oxygen concentrations, which are necessary to support the benthic macrofaunal community responsible for biodiffusion and irrigation. These characteristics support the enhanced solute exchange rates applied in several datasets from these regions. Despite the low bottom water oxygen concentrations in the northern California margin, the significance of enhanced diffusion and NLE in this region suggests that benthic macrofauna are abundant due to the high availability of organic carbon. In the Ceara rise, the decrease of chamber water excess  $[Br^-]$  in deployment CR1 was faster than the molecular diffusive and slightly enhanced rates applied for the other three deployments from this region, despite the low availability of organic carbon in these sediments. The variability in rates and mechanisms of solute exchange used to model tracer datasets in these regions most probably reflects the patchy spatial distribution of benthic macrofaunal populations.

It is possible to detect a trend of increasing benthic oxygen flux with increasing tracer exchange rates by comparing oxygen fluxes from Table 2 with nondiffusive tracer exchange

rates listed in Tables 3 and 5. For example, in the North Carolina slope depocenter, deployments NC1, NC2, NC4, NC5, and NC7 have benthic oxygen fluxes ranging from  $-0.609$  to  $-3.351$  mol m<sup>-2</sup> yr<sup>-1</sup>, with an average of  $-1.824$  mol m<sup>-2</sup> yr<sup>-1</sup>. Tracer datasets for these five deployments were modeled with molecular diffusive solute exchange rates. Benthic O<sub>2</sub> fluxes for NC1 and NC8 to NC13 are slightly higher, ranging from  $-1.139$  to  $-4.934$  mol m<sup>-2</sup> yr<sup>-1</sup> with an average of  $-3.088$  mol m<sup>-2</sup> yr<sup>-1</sup>. Tracer datasets for these five deployments were modeled with enhanced diffusive solute exchange rates ( $2 \leq \varepsilon \leq 78$ ). In the Cape Verde Plateau, benthic oxygen fluxes for CV2 were higher than for CV1. In comparison, the tracer dataset for CV2 required the infNLE model, whereas the CV1 dataset was modeled with molecular diffusive exchange rates. Whereas in these two sites, more significant tracer exchange rates are correlated with higher benthic oxygen flux measurements, trends are less distinct for datasets on the northern California margin and the Ceara Rise as well as between regions.

*Chamber volume and previous benthic solute flux estimates*—Benthic solute fluxes are often derived from the measured decay in chamber water solute concentrations and calculated chamber height estimates according to the following relationship:

$$J = \frac{\partial C}{\partial t} \times CH \quad (6)$$

where  $J$  represents the benthic solute flux (M L<sup>-2</sup> T<sup>-1</sup>),  $\partial C/\partial t$  represents the measured rate of change in chamber water solute concentrations (M L<sup>-3</sup> T<sup>-1</sup>), and  $CH$  represents the chamber height (L). The optimization of model parameters to simulate tracer datasets results in significantly (>20%) higher initial chamber water tracer concentrations, and therefore lower chamber volume and benthic solute flux estimates, than those obtained with linear interpolations of 6 of 22 datasets considered in this work (Fig. 9). This effect is due to the curvature in the decline of simulated chamber water tracer concentrations (Fig. 4 to 8). Note that the curvature in the chamber tracer concentration profile varies with exchange rate and, in the case of NLE, depth of irrigation. Therefore, although evaluating the initial tracer concentration employing a prescribed curve, such as the exponential function applied by Berelson et al. (1998), may offer some improvement, a more accurate evaluation is achieved with an adjustable model of the type described here.

## Discussion

Our results demonstrate the importance of using inert tracers in benthic flux chamber incubations. Tracer loss in excess of that expected by molecular diffusion is indicative of enhanced solute exchange, which significantly alters the extrapolation of chamber water tracer time-series results to initial concentrations. This, in turn, impacts estimates of chamber volume and solute flux.

Although our model cannot be used to predict the spatial extent of irrigation or bioturbation from chamber results, the results in Tables 4 and 5 suggest that, except in cases with the

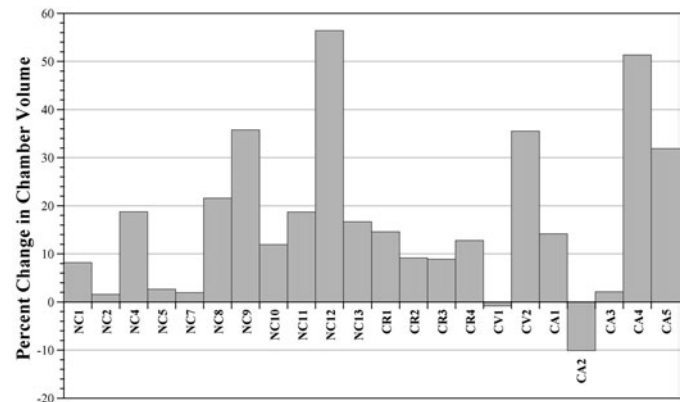


**Fig. 9.** The difference in chamber volume estimated from the solute exchange model relative to that derived by linear extrapolation. Changes in chamber volume correspond to equivalent decreases in calculated benthic solute fluxes.

highest exchange rates, best fit solute exchange and chamber volume parameter values are relatively insensitive to the depth-dependence of nondiffusive solute exchange. Therefore, our results have shown that it is not necessary to have detailed information about the depth-dependence of enhanced solute exchange to estimate solute fluxes from benthic chamber data. Regardless of the depth chosen for enhanced solute exchange, we were able to use the model to (1) distinguish between enhanced diffusive and nonlocal solute exchange, (2) obtain qualitative information from solute exchange parameter values regarding the relative importance of nondiffusive solute exchange in each deployment, and (3) calculate chamber volume.

We report enhanced solute exchange rates in regions with high carbon rain rates, over a wide range of bottom water oxygen concentrations. Furthermore, our results suggest that rates of solute exchange cannot be assumed to be constant, even within relatively short deployments. Solute fluxes across the sediment-water interface may vary in response to changes in macrofaunal activity, due to the depletion of oxygen in chamber water. Future flux incubations should minimize the time interval between tracer injection and sampling while providing sufficient time for the complete homogenization of the tracer in chamber waters.

## References

- Aller, R. C. 1983. The importance of the diffusive permeability of animal burrow linings in determining marine sediment chemistry. *J. Marine Res.* 41:299-322.
- . 1990. Bioturbation and manganese cycling in hemipelagic sediments. *Philos. Trans. Royal Soc. London A* 331:51-68.
- Archer, D., S. Emerson, and C. R. Smith. 1989. Direct measurement of the diffusive sublayer at the deep sea floor using oxygen microelectrodes. *Nature* 340:623-626.

- , and A. Devol. 1992. Benthic oxygen fluxes on the Washington shelf and slope: A comparison of in situ microelectrode and chamber flux measurements. *Limnol. Oceanogr.* 37:614-629.
- Berelson, W. M., M. R. Buchholtz, D. E. Hammond, P. H. Santschi. 1987. Radon fluxes measured with the MANOP bottom lander. *Deep-Sea Res.* 34:1209-1228.
- , D. E. Hammond, C. Fuller. 1982. Radon-222 as a tracer for mixing in the water column and benthic exchange in the southern California borderland. *Earth Planet. Sci. Lett.* 61: 41-54.
- , D. Heggie, A. Longmore, T. Kilgore, G. Nicholson, and G. Skyring. 1998. Benthic nutrient recycling in Port Phillip Bay, Australia. *Estuar. Coast Shelf Sci.* 46:917-934.
- , T. Townsend, D. Heggie, P. Ford, A. Longmore, G. Skyring, T. Kilgore, G. Nicholson. 1999. Modelling bio-irrigation rates in the sediments of Port Phillip Bay. *Marine Freshwater Res.* 50:573-579.
- Boudreau, B. P. 1984. On the equivalence of nonlocal and radial-diffusion models for porewater irrigation. *J. Marine Res.* 42:731-735.
- . 1997. Diagenetic models and their implementation: modelling transport and reactions in aquatic sediments. New York: Springer-Verlag.
- Buchholtz-ten Brink, M. R., G. Gust, and D. Chavis. 1989. Calibration and performance of a stirred benthic chamber. *Deep-sea Res. A* 36:1083-1101.
- Emerson, S., R. Jahnke, and D. Heggie. 1984. Sediment-water exchange in shallow water estuarine sediments. *J. Marine Res.* 42:709-730.
- Glud, R. N., J. K. Gundersen, B. B. Jørgensen, N. P. Revsbech, and H. D. Schulz. 1994. Diffusive and total oxygen uptake of deep-sea sediments in the eastern South Atlantic Ocean: in situ and laboratory measurements. *Deep-sea Res. I* 41: 1767-1788.
- Hammond, D. E., J. McManus, W. M. Berelson, T. E. Kilgore, and R. H. Pope. 1996. Early diagenesis of organic material in equatorial Pacific sediments: stoichiometry and kinetics. *Deep-sea Res. II* 43:1365-1412.
- , H. J. Simpson, G. Mathieu. 1977. Radon 222 distribution and transport across the sediment-water interface in the Hudson River estuary. *J. Geophysical Res.* 82:3913-3920.
- Jahnke, R. A., and M. B. Christiansen. 1989. A free-vehicle benthic chamber instrument for sea floor studies. *Deep-sea Res.* 36:625-637.
- , S. R. Emerson, J. K. Cochran, and D. J. Hirschberg. 1986. Fine scale distributions of porosity and particulate excess  $^{210}\text{Pb}$ , organic carbon and  $\text{CaCO}_3$  in surface sediments of the deep equatorial Pacific. *Earth Planet. Sci. Lett.* 77:59-69.
- , and D. B. Jahnke. 2000. Rates of C, N, P and Si recycling and denitrification at the US Mid-Atlantic continental slope depocenter. *Deep-sea Res. I* 47:1405-1428.
- , and ———. 2004. Calcium carbonate dissolution in deep-sea sediments: Implications of bottom water saturation state and sediment composition. *Geochimica et Cosmochimica Acta.* 68:47-59
- Leslie, B. W., D. E. Hammond, W. M. Berelson, and S. P. Lund. 1990. Diagenesis in anoxic sediments from the California continental borderland and its influence on iron, sulfur, and magnetite behavior. *J. Geophysical Res.* B4, 95:4453-4470.
- Martin, W. R., and G. T. Banta. 1992. The measurement of sediment irrigation rates: A comparison of the  $\text{Br}^-$  tracer and  $^{222}\text{Rn}/^{226}\text{Ra}$  disequilibrium techniques. *J. Marine Res.* 50: 125-154.
- and F. L. Sayles. 1996.  $\text{CaCO}_3$  dissolution in sediments of the Ceara Rise, western equatorial Atlantic. *Geochimica et Cosmochimica Acta* 60:243-263.
- Meile, C., C. M. Koretsky, and P. Van Cappellen. 2001. Quantifying bioirrigation in aquatic sediments: An inverse modeling approach. *Limnol. Oceanogr.* 46:164-177.
- Reimers, C. E. 1987. An in situ microprofiling instrument for measuring interfacial porewater gradients—methods and oxygen profiles from the north Pacific ocean. *Deep-sea Res. A* 34:2019.
- , R. A. Jahnke, and L. Thomsen. 2001. In situ sampling in the benthic boundary layer, p. 245-268. *In* B. P. Boudreau and B. B. Jørgensen [eds.], *The benthic boundary layer: transport processes and biogeochemistry*, Oxford.
- Roychoudhury, A. N., E. Viollier, and P. Van Cappellen. 1998. A plug flow-through reactor for studying biogeochemical reactions in undisturbed aquatic sediments. *Applied Geochem.* 13(2):269-280
- Sayles, F. L., and W. R. Martin. 1995. In situ tracer studies of solute transport across the sediment-water interface at the Bermuda time-series site. *Deep-sea Res. I* 42:31-52.
- Schlüter, M., E. Sauter, H.-P. Hansen, and E. Suess. 2000. Seasonal variations of bioirrigation in coastal sediments: Modelling of field data. *Geochimica et Cosmochimica Acta* 64:821-834.

Submitted 11 June 2003

Revised 30 August 2003

Accepted 18 December 2003